Modern Physics Letters A

NEUTRON STAR MATTER EQUATION OF STATE AND GRAVITATIONAL WAVE EMISSION

OMAR BENHAR

INFN and Department of Physics, Università "La Sapienza", Piazzale Aldo Moro, 2
I-00185 Roma, Italy
benhar@roma1.infn.it

Received (Day Month Year)
Revised (Day Month Year)

The EOS of strongly interacting matter at densities ten to fifteen orders of magnitude larger than the typical density of terrestrial macroscopic objects determines a number of neutron star properties, including the pattern of gravitational waves emitted following the excitation of nonradial oscillation modes. This paper reviews some of the approaches employed to model neutron star matter, as well as the prospects for obtaining new insights from the experimental study of gravitational waves emitted by neutron stars.

Keywords: equation of state; neutron stars; gravitational waves.

PACS Nos.: 04.30-w, 04.30Db, 97.60Jd.

1. Introduction

The equation of state (EOS) is a nontrivial relation linking the thermodynamic variables that specify the state of a physical system[1]. The best known example is Boyle's ideal gas law, stating that the pressure of a collection of N noninteracting, pointlike classical particles, enclosed in a volume V, grows linearly with the temperature T and the average particle density $n = N/V$.

The ideal gas law provides a good description of very dilute systems, in which interaction effects can be neglected. In general, the EOS can be written expanding the pressure, P, in powers of the density (throughout this paper, I will use units such that $\hbar = c = k_B = 1$, k_B being Boltzmann's constant):

$$P = nT \ \left[1 + nB(T) + n^2 C(T) + \ldots\right] \ . \tag{1}$$

The coefficients appearing in the above series, called virial expansion, depend on temperature only, and describe the departure from the ideal gas law arising from interactions. The EOS carries a great deal of dynamical information and provides a link between measurable *macroscopic* quantities, such as pressure and temperature, and the forces acting between the constituents of the system at *microscopic* level.

In this brief review, I will discuss theoretical models of strongly interacting matter at densities up to fifteen orders of magnitude larger than the typical density

of terrestrial macroscopic objects. The EOS in this density regime largely determines neutron star properties, including the pattern of gravitational waves emitted following the excitation of nonradial oscillation modes.

Section 2 provides a summary of neutron star structure, while some of the approaches employed to model neutron star matter are briefly reviewed in Section 3. The dependence of the equilibrium properties of a nonrotating neutron star on the EOS describing matter in its interior is discussed in Section 4. Section 5 is devoted to the analysis of the imprint of the EOS on gravitational wave emission. The conclusions are stated in Section 6.

2. Overview of neutron star structure

The internal structure of a neutron star, whose cross section is schematically illustrated in Fig. 1, is believed to feature a sequence of layers of different composition.

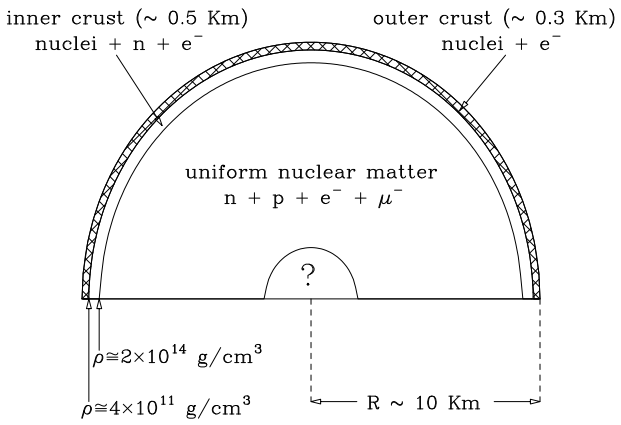

Fig. 1. Schematic illustration of a neutron star cross section. Note that the equilibrium density of uniform nuclear matter corresponds to $\sim 2.7 \times 10^{14}\mathrm{g/cm}^3$.

The outer crust, about 300 m thick with density ranging from $\rho \sim 10^7\mathrm{g/cm}^3$ to the neutron drip density $\rho_d = 4 \times 10^{11}\mathrm{g/cm}^3$, consists of a Coulomb lattice of heavy nuclei immersed in a degenerate electron gas. Moving from the surface toward the interior of the star the density increases, and so does the electron chemical potential. As a consequence, electron capture becomes more and more efficient and neutrons are produced in large number through weak interactions.

At $\rho = \rho_d$ there are no more negative energy levels available to the neutrons, which are therefore forced to leak out of the nuclei. The inner crust, about 500 m thick and consisting of neutron rich nuclei immersed in a gas of electrons and neutrons, sets in. Moving from its outer edge toward the center the density continues to increase, till nuclei start merging to give rise to structures of variable dimensionality, changing first from spheres into rods and eventually into slabs. Finally, at

$\rho \sim 2 \times 10^{14}$g/cm^3, all structures disappear and neutron star matter reduces to a uniform fluid of neutrons protons and leptons in weak equilibrium.

The density of the neutron star core ranges between $\sim 2 \times 10^{14}$ g/cm^3, at the boundary with the inner crust, and a central value that can be as large as $1 - 4 \times 10^{15}$ g/cm^3. Just above 2×10^{14} g/cm^3 the ground state of matter is a uniform fluid of neutrons, protons and electrons. At any given density the fraction of protons, typically less than $\sim 15\%$, is determined by the requirements of weak equilibrium and charge neutrality. At density slightly larger than the equilibrium density of uniform nuclear matter, $\rho_0 \sim 2.7 \times 10^{14}$g/cm^3, the electron chemical potential exceeds the rest mass of the μ meson and the appearance of muons through the the process $n \to p + \mu^- + \overline{\nu}_\mu$ becomes energetically favorable.

All models of EOS based on hadronic degrees of freedom predict that in the density range $\rho_0 \lesssim \rho \lesssim 2\rho_0$ neutron star matter consists mainly of neutrons, with the admixture of a small number of protons, electrons and muons.

This picture may change significantly at larger density, with the appearance of strange baryons produced in weak interaction processes. For example, although the mass of the Σ^- exceeds the neutron mass by more than 250 MeV, its production becomes energetically allowed as soon as the sum of the neutron and electron chemical potentials equals the Σ^- chemical potential.

Finally, as nucleons are known to be composite objects of size $\sim 0.5 - 1.0$ fm, corresponding to a density $\sim 10^{15}$g/cm^3, it is expected that, if the density in the neutron star core reaches this value, matter may undergo a transition to a new phase, in which quarks are no longer clustered into nucleons or hadrons.

3. Models of neutron star matter EOS

It has long been recognized[2] that the Fermi gas model, leading to a simple polytropic EOS, predicts a maximum neutron star mass $\sim 0.7\ M_\odot$, thus dramatically failing to explain the observed neutron star masses[3]. This failure clearly shows that neutron star equilibrium against gravitational colapse requires a pressure other than the degeneracy pressure, whose origin has to be traced back to hadronic interactions. Unfortunately, the need of including dynamical effects in the EOS is confronted with the complexity of the fundamental theory of strong interactions, quantum chromo dynamics (QCD). As a consequence, all available EOS of strongly interacting matter have been obtained within models, based on the theoretical knowledge of the underlying dynamics and constrained, as much as possible, by experimental data.

While the properties of matter in the outer crust can be obtained directly from nuclear data[4], models of the EOS in the inner crust, corresponding to $4 \times 10^{11} < \rho < 2 \times 10^{14}$g/cm^3, are somewhat based on extrapolations of the available empirical information, since the extremely neutron rich nuclei appearing in this density regime are not observed on earth[5].

However, as most of the neutron star mass resides in the core region (typically, the crust olny accounts for less than ~ 2 % of the total mass), the star properties

discussed in this review are largely unaffected by the details of the EOS describing the crust. In what follows, I will only discuss the EOS of neutron star matter in the region of nuclear and supranuclear density, i.e. at $\rho \geq \rho_0 = 2.7 \times 10^{14}\mathrm{g/cm}^3$.

Note that the results described in the following Sections have been obtained under the two standard assumptions, whose validity has long been established[6], that i) thermal effects can be disregarded and ii) neutron star matter is transparent to neutrinos produced in weak interaction processes.

3.1. *Nucleon matter in β-equilibrium*

Models of the EOS of neutron star matter at $\rho_0 \lesssim \rho \lesssim 2-3\rho_0$ rest on the premise that in this density regime nucleons can still be treated as individual particles. This assumption appears to be reasonable, as the shape of the proton charge distribution, obtained by Fourier transforming its measured elelctric form factor, is such that two protons separated by a distance of ~ 1 fm hardly overlap one another.

The EOS of nucleon matter is mainly obtained from two different approaches: nonrelativistic nuclear many-body theory (NMBT) and relativistic mean field theory (RMFT).

In NMBT, nucleon matter is viewed as a collection of pointlike protons and neutrons, whose dynamics is described by the nonrelativistic Hamiltonian

$$H = \sum_i \frac{p_i^2}{2m} + \sum_{j>i} v_{ij} + \sum_{k>j>i} V_{ijk} \ , \tag{2}$$

where m and p_i denote the nucleon mass and the momentum of the i-th particle, respectively, whereas v_{ij} and V_{ijk} describe two- and three-nucleon interactions. The two-nucleon potential, that reduces to the Yukawa one-pion-exchange potential at large distance, is obtained from a fit to the available data on the two-nucleon system, including both deuteron properties and ~ 4000 precisely determined nucleon-nucleon scattering phase shifts[7]. The purely phenomenological three-body term, $V_{ijk} \ll v_{ij}$, is needed to reproduce the binding energies of the three-nucleon bound states[8] and the empirical saturation properties of symmetric nuclear matter[10].

The many-body Schrödinger equation associated with the hamiltonian of Eq.(2) can be solved exactly, using stochastic methods, for nuclei with mass number $A \leq 10$. The energies of the ground and low-lying excited states are in excellent agreement with the experimental data[9]. Accurate calculations can also be carried out for uniform nucleon matter, exploiting translational invariace and using either a variational approach based on cluster expansion and chain summation techniques[10], or G-matrix perturbation theory[11].

Within RMFT, based on the formalism of quantum field theory, nucleons are described as Dirac particles interacting through meson exchange[12]. In the simplest implementation of this approach the dynamics, modeled in terms of a scalar and a vector field[13], is described by the lagrangian density

$$\mathcal{L} = \mathcal{L}_N + \mathcal{L}_M + \mathcal{L}_{int} \ , \tag{3}$$

where

$$\mathcal{L}_N(x) = \bar{\psi}_N(x)\,(i\partial\!\!\!/ - m)\,\psi_N(x)\ , \tag{4}$$

$\psi_N(x)$ denotes the isospin doublet describing the proton and neutron fields and

$$\mathcal{L}_M(x) = -\frac{1}{4}F_{\mu\nu}(x)F^{\mu\nu}(x) + \frac{1}{2}m_\omega^2 V_\mu(x)V^\mu(x) + \frac{1}{2}\partial_\mu\phi(x)\partial^\mu\phi(x) - \frac{1}{2}m_\sigma^2\phi^2(x)\ , \tag{5}$$

with $F_{\mu\nu}(x) = \partial_\nu V_\mu(x) - \partial_\mu V_\nu(x)$. The interaction term is defined in such a way as to give rise to a Yukawa-like meson exchange potential in the static limit:

$$\mathcal{L}_{int}(x) = g_\sigma\phi(x)\bar{\psi}_N(x)\psi_N(x) - g_\omega V_\mu(x)\bar{\psi}_N(x)\gamma^\mu\psi_N(x)\ . \tag{6}$$

In the above equations, $V_\mu(x)$ and $\sigma(x)$ denote the vector and scalar meson fields, respectively, and m_ω, m_σ, g_ω and g_σ are the corresponding masses and coupling constants.

Unfortunately, the equations of motion obtained minimizing the action turn out to be tractable only in the mean field approximation, i.e. replacing the meson fields with their vacuum expectation values, which amounts to treating them as classical fields. Within this scheme the meson masses and coupling constants are determined by fitting the empirical properties of nuclear matter, i.e. binding energy, equilibrium density and compressibility.

NMBT, while suffering from the obvious limitations inherent in its nonrelativistic nature, is strongly constrained by data and has been shown to possess a highly remarkable predictive power. On the other hand, RMFT is based on a very powerful and elegant formalism, but assumes a somewhat oversimplified dynamics, which is not constrained by nucleon-nucleon data. In addition, it is plagued by the uncertainty associated with the use of the mean field approximation, which is long known to fail in strongly correlated systems[14].

Using either NMBT or RMFT one can calculate the energy-density of nucleon matter at any baryon number density n_B and proton fraction x, as well as the proton and nucleon chemical potentials.

The equilibrium conditions with respect to the processes (neutrinos are omitted, as they do not contribute to chemical equilibrium)

$$n \leftrightarrow p + e^-\ \ ,\ \ n \leftrightarrow p + \mu^-\ , \tag{7}$$

obtained from the minimization of the total energy-density, ϵ, subject the constraints of baryon number conservation and charge neutrality, are

$$\mu_n = \mu_p + \mu_e\ \ ,\ \ \mu_e = \mu_\mu \tag{8}$$

and

$$n_p = n_e + n_\mu\ , \tag{9}$$

where $\mu_i = (\partial\epsilon/\partial n_i)_V$ is the chemical potential of the particle of type i ($i = n, p, e, \mu$), whose number density is denoted by n_i. Using the definition of the proton

fraction, $x = n_p/n_B = n_p/(n_n + n_p)$, and exploiting charge neutrality, one can write all chemical potentials as a function of n_B and x. Thus, for any given n_B, x is uniquely determined by Eqs.(8).

Fig. 2 shows the density dependence of the energy per baryon (left panel) and the proton, electron and muon fractions of β-stable matter calculated by Akmal et al.[15] using NMBT. For comparison, the left panel also includes the results corresponding to pure neutron matter ($x = 0$) and symmetric nuclear matter ($x = 1/2$).

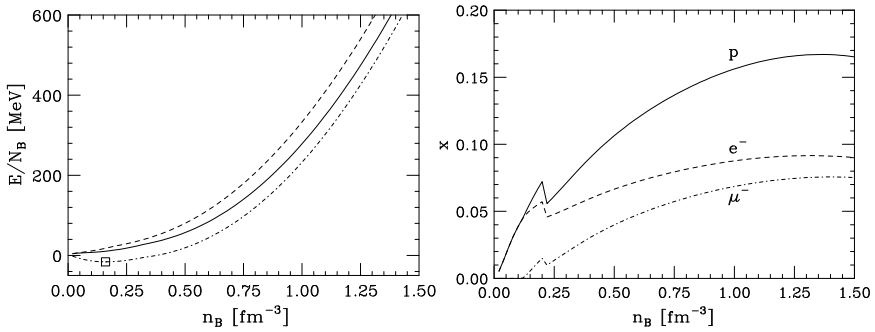

Fig. 2. Left panel: energy per baryon of nucleon matter calculated by Akmal et al.[15], as a function of baryon number density. The dashed, dot-dash and solid lines correspond to pure neutron matter, symmetric nuclear matter and β-stable matter, respectively. The box represents the empirical equilibrium properties of symmetric nuclear matter. Right panel: density dependence of the proton, electron and muon fractions of β-stable matter obtained by Akmal et al.[15].

The EOS in the form $P = P(\epsilon)$ can be readily obtained from the binding energy per baryon shown in Fig. 2 through

$$P = -\frac{1}{n_B^2}\frac{\partial}{\partial n_B}\frac{E}{N_B} \ , \tag{10}$$

and

$$\epsilon = n_B\left(\frac{E}{N_B} + m\right) \ . \tag{11}$$

3.2. *Strange hadronic matter*

As the density increases, different forms of matter, containing hadrons other than protons and neutrons, may become energetically favored. For example, the weak interaction process

$$n + e^- \to \Sigma^- + \nu_e \ , \tag{12}$$

leading to the appearance of a hyperon, sets in as soon as the condition

$$\mu_n + \mu_e = \mu_{\Sigma^-} \tag{13}$$

is fulfilled by the chemical potentials (typically at $n_B \gtrsim 2n_0$, $n_0 = .16$ fm^{-3} being the baryon number density corresponding to equilibrium of symmetric nuclear matter). At larger density the production of Λ's is also energetically allowed.

For any given n_B, the relative aboundances of the different hadronic and leptonic species can be determined from the equations expressing the requirements of equilibrium with respect to weak interactions, conservation of baryon number and charge neutrality.

In principle, both NMBT and RMFT can be generalized to take into account the appearance of hyperons. However, very little is known of their interactions. The available models of the hyperon-nucleon potential[17] are only loosely constrained by few data, while no empirical information is available on hyperon-hyperon interactions.

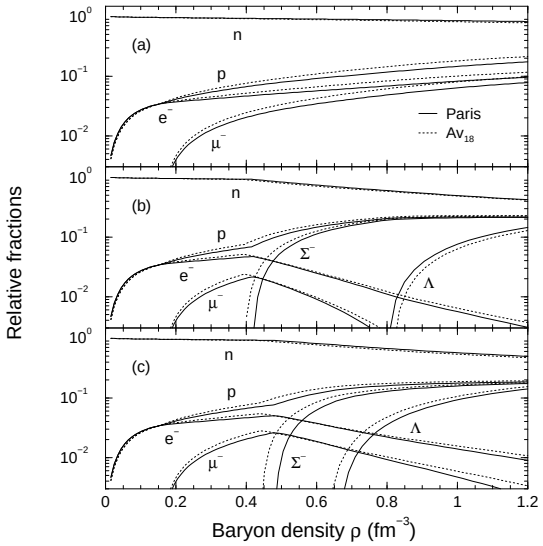

Fig. 3. Composition of neutron star matter calculated by Baldo et al.[16] using G-matrix perturbation theory. Top panel: nucleons and leptons only. Middle panel: nucleons, leptons and noninteracting hyperons (Σ^- and Λ). Lower panel: hyperon-nucleon interaction included. The difference between the solid and dashed lines provides a measure of the model dependence associated with the NN potential v_{ij} (see Eq. (2)).

Fig. 3 shows the composition of neutron star matter resulting from the NMBT calculations of Baldo et al.[16]. Comparison between the middle and lower panel illustrates the role of hyperon-nucleon interactions, modeled using the potential of Maessen et al.[17], whose inclusion pushes the threshold of hyperon production towards larger density. Hyperon-hyperon interactions are neglected altogether.

The transition from nucleon matter to hadronic matter makes the EOS softer, thus leading to a larger compressibility. This feature can be easily understoood, as

processes like the one of Eq. (12) replace particles carrying large Fermi energies with more dilute, and therefore less energetic, strange baryons.

3.3. *Quark matter*

Due to the complexity of QCD, a first principle description of the EOS of quark matter at high density and zero temperature is out of reach of the existing computational approaches. Following the pioneering work of Baym and Chin[18], a number of authors have carried out numerical studies of quark matter based on the simple MIT bag model[19]. Within this model the main features of QCD, namely confinement and asymptotic freedom, are implemented through the assumptions that: i) quarks occur in color neutral clusters confined to a finite region of space (the bag), whose volume is limited by the pressure of the QCD vacuum (the bag constant B), and ii) residual interactions between quarks are weak, and can be treated in low order perturbation theory.

Neglecting quark masses, the bag model EOS, at first order in the color coupling constant α_s, can be obtained in closed form from the relations linking pressure and energy-density to the quark chemical potentials

$$P = \frac{1}{4\pi^2}\left(1-\frac{2\alpha_s}{\pi}\right)\sum_f \mu_f^4 - B \ , \tag{14}$$

and

$$\epsilon = \frac{3}{4\pi^2}\left(1-\frac{2\alpha_s}{\pi}\right)\sum_f \mu_f^4 + B \ , \tag{15}$$

where the sum runs over the active flavors, typically u, d and s, and μ_f is the chemical potential of the quark of flavor f.

For any baryon desity, quark densities are dictated by the requirements of baryon number conservation, charge neutrality and weak equilibrium. In the case of three active flavors one finds

$$n_B = \frac{1}{3}(n_u + n_d + n_s) \quad , \quad \frac{2}{3}n_u - \frac{1}{3}n_d - \frac{1}{3}n_s - n_e = 0 \tag{16}$$

and

$$\mu_d = \mu_s = \mu_u + \mu_e \ . \tag{17}$$

Note that in the above equations the possible appearance of μ mesons is not taken into account, as the results of numerical calculations show that the electron chemical potential never exceeds the muon mass.

Fig. 4 shows the composition of charge neutral quark matter in weak equilibrium. obtained from the MIT bag model. The calculations have been carried out including massless u and d quarks and strange quarks of mass $m_s = 150$ MeV, and setting $B = 200$ MeV/fm^3 and $\alpha_s = 0.5$. It appears that at large densities quarks of the three different flavors are present in equal number, and leptons are no longer needed to guarantee charge neutrality.

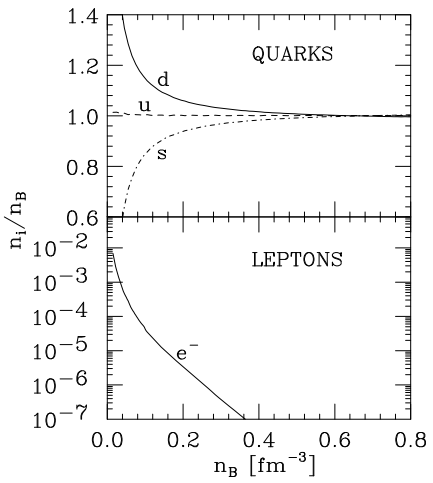

Fig. 4. Composition of charge neutral matter of u, d and s quarks and electrons in weak equilibrium, obtained from the MIT bag model setting $m_u = m_d = 0$, $m_s = 150$ MeV, $B = 200$ MeV/fm^3 and $\alpha_s = 0.5$.

4. EOS and properties of nonrotating neutron stars

Plugging the EOS, $P = P(\epsilon)$, into the Tolman Oppenheimer Volkoff (TOV) equations[20,2]

$$\frac{dP(r)}{dr} = -G\,\frac{[\epsilon(r)+P(r)]\left[M(r)+4\pi r^2 P(r)\right]}{r^2\,[1-2GM(r)/r]}\ , \tag{18}$$

where G denotes the gravitational constant, and

$$M(r) = 4\pi\int_0^r r'^2 dr'\epsilon(r')\ , \tag{19}$$

one can obtain the properties of stable nonrotating neutron stars. Eqs. (18) and (19) are solved by integrating outwards with the initial condition $\epsilon(r=0)=\epsilon_c$. For any given value of the central density, ϵ_c, the star radius R is determined by the condition $P(R)=0$ and its mass $M = M(R)$ is given by Eq. (19).

Plotted as a function of central density, the neutron star mass exhibits a maximum, whose value M_{max} is mostly determined by the stiffness of the EOS. Stiffer EOS, corresponding to more incompressible neutron star matter, lead to larger M_{max}. Therefore, in principle, measurements of neutron star masses may be used to constrain the models of EOS at $\rho > \rho_0$.

Unfortunately, comparison of the calculated M_{max} with the neutron star masses obtained from observations, ranging between ~ 1.1 and $\sim 1.9\ M_\odot$[3,21], does not provide a stringent test on the EOS, as most models predict a stable star configuration with mass compatible with the data. A stronger constraint may soon come from measurements of the neutron star mass-radius ratio. It has been recently reported[22] that the Iron and Oxygen transitions observed in the spectra of 28 bursts of the

X-ray binary EXO0748-676 correspond to a gravitational redshift $z = 0.35$, yielding in turn a mass-radius ratio of the source $M/R = 0.153\ M_\odot/\mathrm{km}$.

The results of Cottam et al.[22] are still somewhat controversial and need to be confirmed. However, Fig. 5 shows that the $M(R)$ relations corresponding to EOS obtained from NMBT including only nucleon degrees of freedom are consistent with the redshift measurement. The possible appearance of deconfined quark matter in a small region in the center of the star does not dramatically change the picture[24], while the occurrence of a transition to hyperonic matter at densities as low as twice the equilibrium density of nuclear matter seems to be ruled out[32]. From Fig. 5 it also appears that none of the considered EOS, all of them obtained from nonrelativistic NMBT, predicts a $M(R)$ curve extending into the region, forbidden by causality, in which the speed of sound in matter exceeds the speed of light[23].

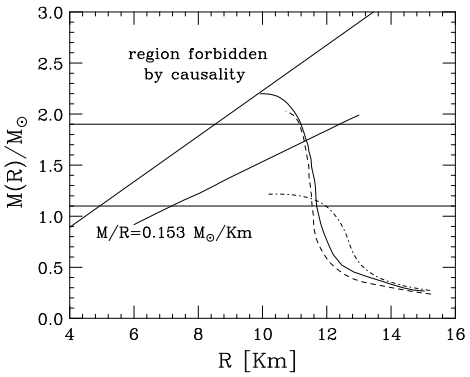

Fig. 5. Mass radius relation for different EOS. Solid line: nucleons only[10]. Dotdash: nucleons and hyperons[16]. Dashes: nucleons and deconfined quarks[24]. The horizontal lines denote the observational limits on the neutron star mass, whereas the other straight lines correspond to the gravitational redshift measurement of Cottam et al.[22] and to the boundary of the region forbidden by causality.

5. Gravitational waves from neutron stars

When a neutron star is perturbed by some external or internal event, it can be set into non radial oscillations, emitting gravitational waves at the charateristic frequencies of its quasi-normal modes. This may happen, for example, as a consequence of a glitch, a close interaction with an orbital companion, a phase transition occurring in its inner core or in the aftermath of a gravitational collapse. The frequencies and damping times of the quasi-normal modes carry information on the structure of the star and the properties of matter in its interior.

Quasi-normal modes are classified according to the source of the restoring force which prevails in bringing the perturbed element of fluid back to the equilibrium position. Thus, we have a g-mode if the restoring force is mainly provided by buoyancy,

or a p-mode if it is due to a gradient of pressure. The frequencies of the g-modes are lower than those of the p-modes, the two sets being separated by the frequency of the fundamental f-mode, associated with global oscillations of the fluid. General relativity also predicts the existence of additional modes, called w-modes, which are purely gravitational, as they do not induce fluid motion[25,26]. The w-modes can be both polar (even parity) and axial (odd parity). They are highly damped and, in general, their frequencies are higher than the p-mode frequencies.

To see an example of how the oscillation frequencies of quasi-normal modes depend on the neutron star matter EOS, consider the axial w-modes of a nonrotating star. In this case, the complex frequencies are eigenvalues of a Schrödinger-like equation whose potential $V_\ell(r)$ explicitely depend upon the EOS according to[27]

$$V_\ell(r) = \frac{\mathrm{e}^{2\nu(r)}}{r^3}\ \left\{\ell(\ell+1)r + r^3\left[\epsilon(r) - P(r)\right] - 6M(r)\right\}\ , \tag{20}$$

where

$$\frac{d\nu}{dr} = -\frac{1}{\left[\epsilon(r)+P(r)\right]}\frac{dP}{dr}\ . \tag{21}$$

Using a set of different EOS one obtains strongly damped eigenmodes[28], whose frequencies exhibit the behavior displayed in Fig. 6.

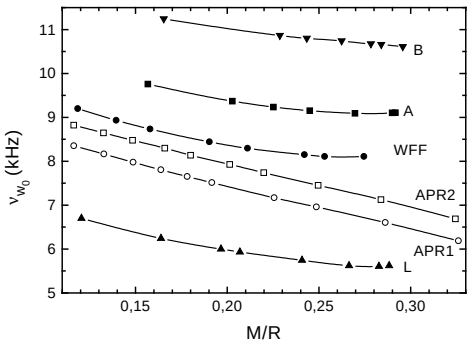

Fig. 6. Frequencies of the first axial w-mode of a nonrotating neutron star, plotted as a function of the star compactness. The different curves correspond to different models of EOS[28].

The pattern emerging from Fig. 6 strictly reflects the stiffness of the different EOS in the relevant density region (typically $\rho_0 < \rho < 5\rho_0$), softer EOS corresponding to higher frequencies. For example, the curve labelled B has been obtained from a model based on NMBT and including strange baryons[29], which leads to a very soft EOS and a maximum mass of $\sim 1.4\ M_\odot$. On the other hand, the curve labelled L corresponds to a RMFT calculation including nucleons only[30], yielding a maximum mass of $\sim 2.7\ M_\odot$.

In 1998, Andersson and Kokkotas[31] computed the frequencies of the f-mode, the first p-mode and the first polar w-mode of a non rotating neutron star for a

number of EOS available at that time. They fitted the results of their calculations with appropriate *universal functions* of the macroscopic properties of the star, i.e. mass and radius, and showed how these empirical relations could be used to put constraints on these quantities if the frequency of one or more modes could be identified in a detected gravitational signal.

A similar analysis has been recently carried out by Benhar et al.[32], who have included in their fit results obtained from state-of-the art EOS. As an example, Fig. 7 shows the frequencies of the fundamental mode corresponding to different EOS, plotted as as a function of the square root of the average density. It appears that the frequencies corresponding to different EOS tend to *scale* to a straight line. The sizable displacement ($\sim$ 100 Hz) of the scaling line of Benhar et al. (thick solid straight line), with respect to the one obtained by Andersson and Kokkotas[31] (dashed straight line), reflects more than a decade of improvements of theoretical models of the EOS.

The damping time of the f-mode and the frequencies and damping times of the p- and w-modes also exhibit scaling, when plotted as a function of the compactness (M/R). As a consequence, as pointed out by Anderson and Kokkotas[31,33], identification of the frequency and damping time of some of these modes in a detected gravitational signal would allow one to determine the radius of the source knowing its mass.

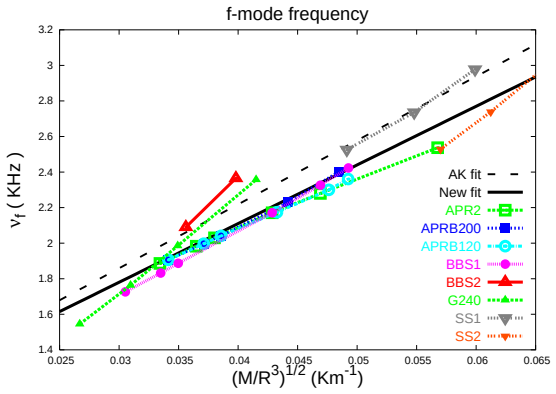

Fig. 7. Frequency of the f-mode plotted as a function of the square root of the average density for different EOS[32]. The fits of Andersson and Kokkotas[31] and Benhar et al.[32] are labelled AK fit and New fit, respectively.

In addition to carrying out the analysis proposed by Anderson and Kokkotas[31,33], one may want to address a different, more direct, question. Will the simultaneous knowledge of the mode frequencies and the mass of the star, its only accurately measured observable, provide a severe test to discriminate among different EOS?

As an example, let us consider the fundamental mode. Numerical simulations

show that this is the mode which is mostly likely to be excited in many astrophysical processes and its damping time is quite long, so that it should appear as a sharp peak in the spectrum of the gravitational signal.

Figure 8 shows the mass dependence of the f-mode frequencies obtained from the EOS models included in the analysis of Benhar et al.[32].

Comparison between the curve labelled APR2 and those labelled APRB120 and APRB200 indicates that the presence of quark matter in the star inner core does not significantly affect the pulsation properties of the star. This is a general feature, also observed in the behavior of p- and w-modes.

The BBS1 and APR2 EOS, based on similar dynamical models, turn out to yield appreciably different f-mode frequencies. This is likely to be ascribed to the effect of the relativistic corrections included in the APR2 EOS and to different treatments of three-nucleon interactions.

The transition to hyperonic matter, predicted by the BBS2 model, produces a sizable softening of the EOS, thus leading to stable neutron star configurations of very low mass. As a consequence, the corresponding f-mode frequency is significantly higher than those obtained from the other models. So much higher, in fact, that its detection would provide a clear signature of the presence of hyperons in the neutron star core.

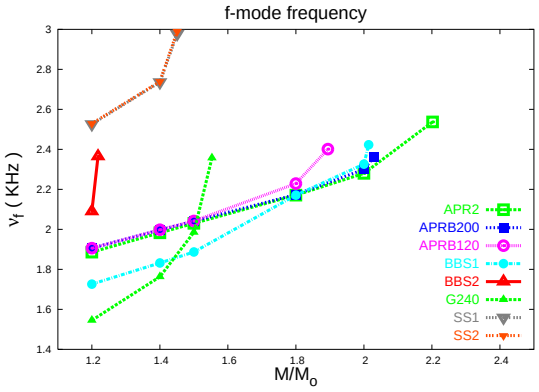

Fig. 8. Frequency of the f-mode, plotted as a function of the mass of the emitting star for different models of EOS[32].

It is also interesting to compare the f-mode frequencies corresponding to models BBS2 and G240, as they both predict the occurrence of strange baryons but are obtained from different theoretical approaches, NMBT and RMFT, based on different descriptions of the underlying dynamics. The behavior of ν_f displayed in Fig. 8 directly reflects the relations between mass and central density obtained from the two EOS, larger frequencies being always associated with larger densities. For example, the configurations of mass $\sim 1.2\ M_\odot$ obtained from the G240 and BSS2 have central densities $\sim 7{\times}10^{14}$ g/cm^3 and $\sim 2.5{\times}10^{15}$ g/cm^3, respectively. On the

other hand, the G240 model requires a central density of $\sim 2.5\times10^{15}$ g/cm^3 to reach a mass of $\sim 1.55\ M_\odot$ and a consequent ν_f equal to that of the BBS2 model.

The curves labelled SS1 and SS2 correspond to *strange stars*, entirely made of quark matter with equal number of up, down and strange quarks. The peculiar properties of these stars, which are also apparent in the mass-radius relation, largely depend on their being self-bound objects[34,35].

6. Conclusions

The results briefly reviewed in Section 5 suggest that the observation of gravitational waves emitted by neutron stars may provide valuable new insight, allowing one to severely constrain theoretical models of strongly interacting matter at high density and zero temperature.

To address the question of whether the existing gravitational antennas may actually be able to detect these signals let us consider, as an example, a neutron star of mass $M = 1.4\ M_\odot$ described by the EOS of Akmal et al.[15], and assume that its fundamental mode (whose frequency and damping time are $\nu_f = 1983\ Hz$ and $\tau_f = 0.184\ s$, respectively[32]) has been excited by some external or internal event. The signal emitted by the star can be modeled as a damped sinusoid[36]

$$h(t) = \mathcal{A} e^{(t_{\rm arr}-t)/\tau_f} \sin\left[2\pi\nu_f\,(t-t_{\rm arr})\right]\ , \tag{22}$$

where $t_{\rm arr}$ is the arrival time and $\mathcal{A}$ is the mode amplitude. The energy stored into the mode can be estimated by integrating the energy flux

$$\frac{dE_{\rm mode}}{dSd\nu} = \frac{\pi}{2}\,\nu^2\,|\,\tilde{h}(\nu)\,|^2, \tag{23}$$

where $\tilde{h}(\nu)$ is the Fourier transform of $h(t)$, over surface (S) and frequency (ν).

The signal to noise ratio (SNR) can be expressed in terms of $\tilde{h}(\nu)$ and the noise power spectral density of the detector, $S_n(\nu)$. In the case of the ground based interferometric antenna VIRGO[37] one finds that SNR=5 corresponds to $E_f \sim 6\times10^{-7}\ M_\odot$ for a source in our Galaxy (distance from Earth $d \sim 10$ kpc) and $E_f \sim 1.3\ M_\odot$ for a source in the VIRGO cluster ($d \sim 15$ Mpc). Similar estimates can be found for the detectors LIGO, GEO and TAMA.

These numbers suggest that it is unlikely that the first generation of interferometric antennas will detect gravitational waves emitted by an oscillating neutron star. However, detection will become possible with the next generation of detectors, which are expected to be much more sensitive at frequencies above 1-2 kHz.

Identification of the modes in a detected signal, combined with the knowledge of the mass of the emitting star will provide critical new information on its internal structure, thus opening the era of *gravitational wave asteroseismology*.

Acknowledgments

This brief review is based on a talk given at the W.K. Kellog Radiation Laboratory, California Institute of Technology, whose hospitality is gratefully acknowledged.

The results discussed in Sections 4 and 5 have been obtained in collaboration with E. Berti, V. Ferrari, L. Gualtieri and R. Rubino.

References

1. K. Huang *Statistical Mechanics* (Wiley, New York, 1963).
2. J.R. Oppenheimer and G.M. Volkoff, *Phys. Rev.* **55**, (1939) 374.
3. S.E. Thorsett and D. Chakrabarty, *ApJ* **512**, 288 (1999).
4. G. Baym, C.J. Pethick and P. Sutherland, *ApJ* **170**, 299 (1971).
5. C.J. Pethick, B.G. Ravenhall and C.P. Lorenz, *Nucl. Phys.* **A584**, 675 (1995).
6. S.L. Shapiro and S.A. Teukolsky, *Black Holes, White Dwarfs and Neutron Stars* (Wiley, New York, 1983).
7. R.B. Wiringa, V.G.J. Stoks and R. Schiavilla, *Phys. Rev. C* **51**, 38 (1995).
8. B.S. Pudliner, V.R. Pandharipande, J. Carlson, S.C. Pieper and R.B. Wiringa, *Phys. Rev. C* **56**, 1720 (1995).
9. S.C. Pieper and R.B. Wiringa, *Ann. Rev. Nucl. Part. Sci.* **51**, 53 (2001).
10. A. Akmal and V. R. Pandharipande, *Phys. Rev. C* **56**, 2261 (1997).
11. M. Baldo, G. Giansiracusa, U. Lombardo and H.Q. Song, *Phys. Lett.* **B473**, 1 (2000).
12. B.D. Serot and J.D. Walecka, *Adv. Nucl. Phys.* **16**, 1 (1986).
13. J.D. Walecka, *Ann. Phys.* **83**, 491 (1974).
14. L.P. Kadanoff and G. Baym, *Quantum Statistical Mechanics* (Benjamin, New York, 1972).
15. A. Akmal, V.R. Pandharipande and D.G. Ravenhall, *Phys. Rev. C* **58**, 1804 (1998).
16. M. Baldo, G.F. Burgio and H.-J. Schulze, *Phys. Rev. C* **61**, 055801 (2000).
17. P.M.M. Maessen, T.A. Rijken and J.J. deSwart, *Phys. Rev. C* **40**, 2226 (1989).
18. G. Baym and S.A. Chin, *Phys. Lett.* **B62**, 241 (1976).
19. A. Chodos, R.L. Jaffe, K. Johnson, C.B. Thorne and V.F. Weiskopf, *Phys. Rev. D* **9**, 3471 (1974).
20. R.C. Tolman, *Relativity, Thermodynamics and Cosmology*, (Oxford University Press, 1934)
21. H. Quaintrell, *et al.*, *A&A*, **401**, 303 (2003).
22. J. Cottam *et al*, *Nature*, **420**, 51 (2002).
23. J.M. Lattimer and M. Prakash, *ApJ*, **550**, 426 (2001).
24. O. Benhar and R. Rubino, *A&A*, **434**, 247 (2005).
25. S. Chandrasekhar and V. Ferrari, *Proc. R. Soc. Lond.*, **A434**, 449 (1991).
26. K.D. Kokkotas and B.F. Schutz, *MNRAS*, **255**, 119 (1992).
27. S. Chandrasekhar and V. Ferrari, *Proc. R. Soc. London*, **A432**, 247 (1991).
28. O. Benhar, E. Berti and V. Ferrari, *MNRAS* **310**, 797 (1999).
29. V.R. Pandharipande, *Nucl. Phys.* **A178**, 123 (1971).
30. V.R. Pandharipande and R.A. Smith, *Phys. Lett.* **B59**, 15 (1975).
31. N. Andersson and K.D. Kokkotas, *MNRAS*, **299**, 1059 (1998).
32. O. Benhar, V. Ferrari and L. Gualtieri, *Phys. Rev. D*, **70**, 124015 (2004)
33. N. Andersson and K.D. Kokkotas, *MNRAS*, **320**, 307 (1999).
34. A.R. Bodmer, *Phys. Rev. D*, **4**, 1601 (1971).
35. E. Witten, *Phys.Rev. D*, **30**, 272 (1984).
36. V. Ferrari, G. Miniutti and J. A. Pons, *Class. Quant. Grav.*, **20**, 8841 (2003).
37. T. Damour, B. R. Iyer and B. S. Sathyaprakash, *Phys. Rev. D* **57**, 885 (1998).